

Article

Dynamic Decoupling Method Based on Motor Dynamic Compensation with Application for Precision Mechatronic Systems

Kaixin Liu ¹, Yang Liu ^{2,*}, Fazhi Song ² and Jiubin Tan ²

¹ Department of Control Science and Engineering, Harbin Institute of Technology, Harbin 150001, China; 19b904023@stu.hit.edu.cn

² Center of Ultra-Precision Optoelectronic Instrument Engineering, Harbin Institute of Technology, Harbin 150001, China; fazhsong@hit.edu.cn (F.S.); jbtan@hit.edu.cn (J.T.)

* Correspondence: hitlg@hit.edu.cn

Abstract: Motors are widely employed in mechatronic systems, especially in precision multiple degrees of freedom motion systems. In most applications, the dynamic equation between the motor instruction and the actual driving force is simplified as a constant. Subsequently, the static decoupling method can be utilized to design the feedback controller. However, in high-precision mechatronic systems, motor dynamics cannot be neglected, and the static decoupling performance is compromised due to discrepancies between motors. In this paper, a dynamic decoupling method is developed to improve the decoupling performance of the multiple-input multiple-output systems. The effects of transmission delays, motor dynamics, and discrepancies between different motors are taken into consideration in the dynamic decoupling method. Furthermore, a data-driven optimization method is developed to estimate the parameters of the dynamic decoupling controller. The effectiveness and superiority of the proposed method are demonstrated through numerical simulations. The experimental results show that the dynamic decoupling control method can achieve a 97.75% performance improvement at least compared to the static decoupling control method.

Keywords: data-driven; dynamic decoupling control; motors; multiple-input multiple-output (MIMO) systems



Citation: Liu, K.; Liu, Y.; Song, F.; Tan, J. Dynamic Decoupling Method Based on Motor Dynamic Compensation with Application for Precision Mechatronic Systems. *Energies* **2024**, *17*, 2038. <https://doi.org/10.3390/en17092038>

Academic Editor: Daniel Morinigo-Sotelo

Received: 12 March 2024

Revised: 3 April 2024

Accepted: 10 April 2024

Published: 25 April 2024



Copyright: © 2024 by the authors. Licensee MDPI, Basel, Switzerland. This article is an open access article distributed under the terms and conditions of the Creative Commons Attribution (CC BY) license (<https://creativecommons.org/licenses/by/4.0/>).

1. Introduction

Multiple degrees of freedom (DoFs) mechatronic systems play a pivotal role in various industrial applications, such as robot manipulators [1], vibration test systems [2], numerical control machine tools [3], applications in the field of energy [4], etc. The parallel design scheme, owing to its spatial and dynamic advantages, is widely adopted in these systems [5]. However, the inherent simplicity of this design introduces challenges, particularly in control aspects, which become more pronounced in applications to achieve high-precision motion, such as the wafer scanner utilized in lithography equipment [6].

To obtain high-precision performance for each degree of freedom (DOF), numerous control strategies have been developed [7], and the decoupling control method emerges as the most widely employed approach. Based on the mechanical structure and operating under the rigid body hypothesis, a static decoupling matrix can be established to effectively decouple the motion of each DOF [8]. Nevertheless, three significant challenges arise in high-precision motion scenarios. Firstly, the static decoupling matrix, which is employed for achieving rigid body decoupling, relies on mechanical structure parameters, including the positions of the center of mass (CoM) and the stress point. Owing to the impact of machining and assembly errors, discrepancies may arise between the utilized parameters and their actual values, resulting in static decoupling errors [9]. Secondly, to achieve high-performance motion in mechatronic systems, high-performance motors, such as

linear motors, voice coil motors, and piezoelectric ceramic motors, are often employed as actuators [10]. In the static decoupling method, the characteristics of each motor are considered to be consistent and unchanging during motion. However, owing to variations between different motors and drivers, as well as limitations in magnetic field strength and current loop bandwidth [11], the static decoupling method cannot achieve complete decoupling in essence. Therefore, the decoupling performance of the static decoupling method is compromised. Thirdly, the varying transmission delays across different channels further exacerbate the decoupling effect [12]. Owing to the influences of these factors, the decoupled system using a static decoupling matrix does not exhibit a diagonal form, leading to the emergence of interactions among degrees of freedom, commonly known as cross-talk [13,14]. With increasing accuracy requirements, cross-talk has become a significant impediment to achieving the desired performance in precision mechatronic systems [15].

To eliminate the cross-talk and improve the decoupling performance, various methods have been reported in the literature, which can be categorized into two main approaches. The first approach treats cross-talk as a parasitic dynamic of each DOF, allowing the design of a robust feedback controller to suppress its effects [16]. The most prevalent method within this category is the equivalent transfer function (ETF) method [17]. In the ETF method, the plant to be controlled in each loop is represented by a generalized model when other loops are closed [18]. It is evident that the interactions are taken into account, therefore, a better feedback controller can be designed for improved performance. However, because the generalized plant of each DoF incorporates the influence of controllers from other DoFs, it is complicated to refine the controller when the performance requirement is not satisfied. In [19], an ETF method is proposed, in which the complicated interaction modes are approximated as lower-order equivalent models to simplify the design of the controller. In addition to the ETF method, other robust control methods can be utilized such as the hybrid integrator–gain method, the H_∞ method, the model predictive control method, etc. [20]. However, since the interactions inevitably increase the complexity of the plant and reduce the attainable bandwidth, only a limited reduction of cross-talk can be obtained. Consequently, the second method, which directly improves the accuracy of decoupling, proves to be the more effective approach in enhancing the performance of precision mechatronic systems.

As highlighted earlier, interactions, stemming from errors in mechanical parameters, variations between motors, and transmission delays, can compromise system performance. Consequently, it becomes imperative to compensate for these factors to achieve full decoupling. Conventionally, mechanical parameters can be calibrated using professional instruments to enhance the accuracy of the static decoupling matrix [21]. However, due to limitations in workspace, certain instruments may no longer be suitable [22]. Furthermore, this indirect optimization method may introduce additional calculation errors in the process. Due to the influence of the other two factors, it can be noted that achieving full decoupling of the system with a static decoupling matrix becomes impractical. Based on the compensation for the inconsistency of motors and transmission channels, a dynamic decoupling controller is proposed in this paper. The dynamic decoupling controller consists of two components: a dynamic component parameterized as a rational transfer function, and a static component. The dynamic component is employed to address inconsistencies between motors and transmission channels, while the static component is utilized to achieve full decoupling of the rigid body of the mechatronic system.

Additionally, to obtain the optimal estimate of the unknown parameter in the dynamic decoupling controller, a data-driven optimization method is developed in this paper, which is inspired by the virtual reference feedback tuning (VRFT) method [23]. The key contributions of this work, in comparison to existing literature, can be succinctly outlined as follows:

- (1) A dynamic decoupling control method is established in this paper, based on the compensation for the motor dynamics and the transmission delays.
- (2) A data-driven optimization method is developed in this paper to estimate the unknown parameters of the dynamic decoupling controller, requiring only minimal

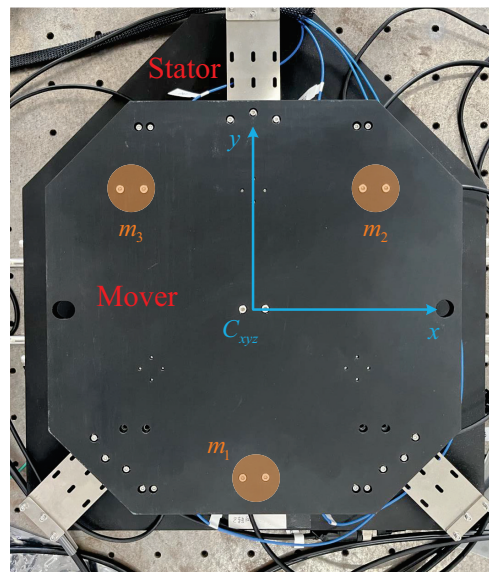
model information. Furthermore, the proposed method is non-iterative, necessitating only a single experiment.

Notations: Let R be the set of real numbers. For n , a positive integer, R^n is the set of real vectors of dimension n . Vector $x \in R^n$ denotes $[x_1, \dots, x_n]^T$. For a vector $x_c \in R^n$, the i -th element can be denoted as $x_{c,i}$. We define $\|\cdot\|_2$ as the l_2 norm of vectors, i.e., $\|x\|_2 = (\sum_{i=1}^n x_i^2)^{1/2}$.

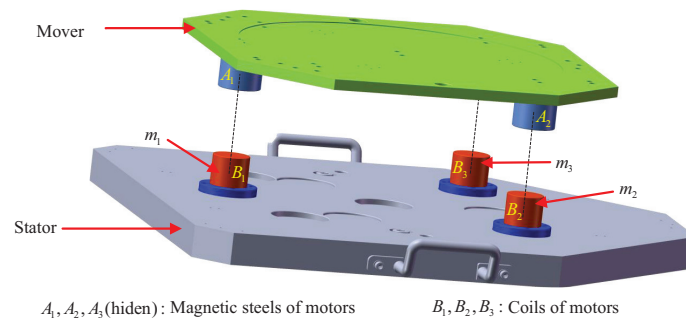
2. Problem Formulation

2.1. Control Configuration of the Multiple DoFs Mechatronic System

We consider a precision multiple DoFs mechatronic system, as depicted in Figure 1, which is a prototype for the short stroke stage of the wafer stage. The prototype shown in Figure 1 consists of a stator and a mover with sufficient stiffness. The mover is driven by three voice coil motors labeled as m_1 , m_2 , and m_3 , respectively, to accomplish nano-scale motion. The voice coil motor can achieve precise and linear motion with high acceleration and high force-to-weight ratio, which render it ideal for applications that require fast and accurate positioning. Three linear encoders are mounted close to the motors; for simplicity, the measurement data of the encoders are supposed to be equal to the displacement distance of the voice coil motors. The target point, defined as the center point of the mover, is controlled to track a predetermined trajectory. The reference trajectory is defined in a Cartesian coordinate system, denoted as C_{xyz} , and the displacements of the three degrees of freedom of the target point can be directly obtained as y_z , y_{θ_x} , and y_{θ_y} , respectively.



(a) Overhead view of the prototype.



A_1, A_2, A_3 (hidden): Magnetic steels of motors B_1, B_2, B_3 : Coils of motors

(b) Detailed mechanical structure drawing of the prototype.

Figure 1. The diagram of the prototype of the short stroke stage.

To control the prototype, the decoupling control scheme based on a nominal static decoupling matrix can be utilized, as Figure 2 shows. In this configuration, $P(s) \in \mathbb{C}^{3 \times 3}$ is the rigid body dynamics model of the mover describing the relationship between the motor driving force and the displacement of the target point. $P_m(s) \in \mathbb{C}^{3 \times 3}$ represents the transfer function between motor instruction and motor driving force, which is in the form of a diagonal. $P_t(s) \in \mathbb{C}^{3 \times 3}$ is denoted as a transmission delays matrix of three transmission channels from the digit controller to drivers. $K \in \mathbb{R}^{3 \times 3}$ is the static decoupling matrix to decouple the plant $P(s)$. $C(s) \in \mathbb{C}^{3 \times 3}$ is the diagonal feedback controller matrix comprised of single-input single-output controllers designed with respect to the desired decoupled system. The signals $r(t) \in \mathbb{R}^3$ and $e(t) \in \mathbb{R}^3$ are a high-order polynomial trajectory and tracking error, respectively. $u(t) \in \mathbb{R}^3$ is the control signal calculated by $C(s)$. $f_c(t) \in \mathbb{R}^3$ and $f(t) \in \mathbb{R}^3$ represent the motor instruction and the actual driving force of the motor. $y(t) \in \mathbb{R}^3$ is the measured displacement of the target point in coordinate C_{xyz} . In addition, the displacements of three voice coil motors can be denoted as $y_v(t) \in \mathbb{R}^3$, which is not represented in the block diagram. Based on the definitions above, the dynamic model of the control system can be described as follows:

$$\begin{cases} y(t) = P(s)f(t) \\ f(t) = P_m(s)P_t(s)f_c(t) \\ f_c(t) = Ku(t) \\ u(t) = C(s)e(t) \\ e(t) = r(t) - y(t) \end{cases} \quad (1)$$

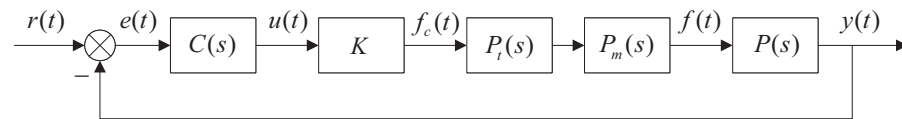


Figure 2. The configuration of the decoupling control.

2.2. Description of Nominal Static Decoupling Method

To simplify the controller design, the nominal static decoupling method can be primarily used to stabilize the system. In the static decoupling method, the transmission delays and the motor dynamics are neglected so that $P_t(s) = I$ and $P_m(s) = \alpha I$, where I is the identity matrix. The simplified structure of the prototype is shown in Figure 3a, with the nominal mechanical parameters known. From Figure 3a, it can be concluded that the CoM coincides with the target point and the distances between motors and the CoM in the coordinate C_{xyz} are $(0, -l_1)$, (l_2, l_1) , and $(-l_2, l_3)$, respectively. Under the rigid body hypothesis, the dynamic equations of the motion of the target point can be established as

$$\begin{cases} m\ddot{y}_z = f_1 + f_2 + f_3 \\ J_x\ddot{\theta}_x = -l_1f_1 + l_3f_2 + l_3f_3 \\ J_y\ddot{\theta}_y = -l_2f_2 + l_2f_3 \end{cases} \quad (2)$$

where f_1 , f_2 , and f_3 are driving forces of three motors, respectively. m is the mass of the mover. J_x and J_y are moment of inertia of θ_x and θ_y at the CoM, respectively. From (2), $P(s)$ can be modeled as

$$P(s) = \begin{bmatrix} \frac{1}{ms^2} & \frac{1}{ms^2} & \frac{1}{ms^2} \\ -\frac{l_1}{J_x s^2} & \frac{l_3}{J_x s^2} & \frac{l_3}{J_x s^2} \\ 0 & -\frac{l_2}{J_y s^2} & \frac{l_2}{J_y s^2} \end{bmatrix}. \quad (3)$$

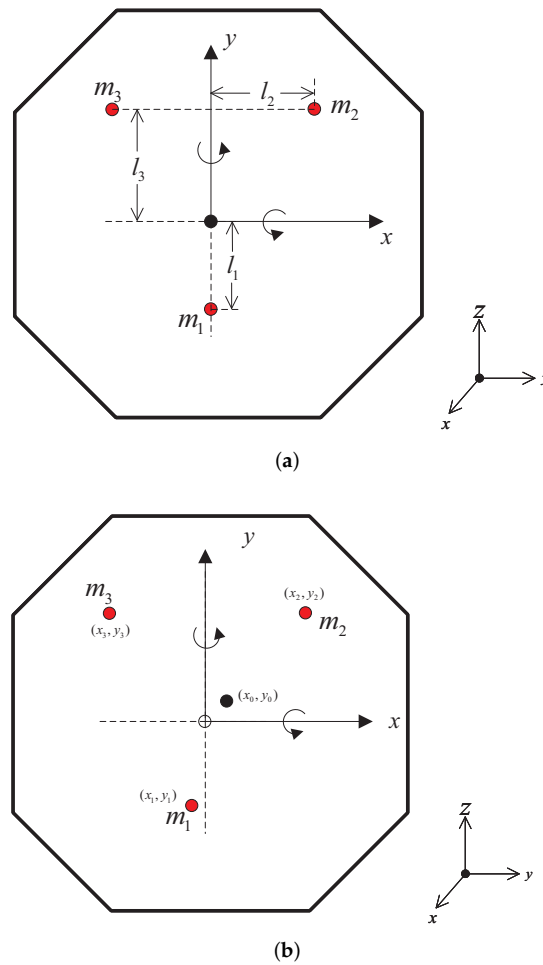


Figure 3. The simplified structure diagrams of the prototype with (a) nominal mechanical parameters and (b) actual mechanical parameters.

It is evident that $P(s)$ is a multivariable system and is not in diagonal form. Directly designing an appropriate feedback controller for such a system is challenging. To apply the static decoupling method, a static decoupling matrix should be employed. Based on the nominal model $P(s)$, the nominal static decoupling matrix can be determined easily as follows:

$$K = \begin{bmatrix} \frac{l_3}{l_1+l_3} & -\frac{1}{l_1+l_3} & 0 \\ \frac{l_1}{2(l_1+l_3)} & \frac{1}{2(l_1+l_3)} & -\frac{1}{2l_2} \\ \frac{l_1}{2(l_1+l_3)} & \frac{1}{2(l_1+l_3)} & \frac{1}{2l_2} \end{bmatrix}. \tag{4}$$

Consequently, the decoupled system achieves full decoupling, which can be written as

$$\begin{aligned} D(s) &= P(s)K \\ &= \begin{bmatrix} \frac{1}{ms^2} & 0 & 0 \\ 0 & \frac{1}{J_x s^2} & 0 \\ 0 & 0 & \frac{1}{J_y s^2} \end{bmatrix}. \end{aligned} \tag{5}$$

Subsequently, three single-input single-output (SISO) feedback controllers, such as PID controllers, can be easily designed with respect to $1/ms^2$, $1/J_x s^2$, and $1/J_y s^2$. However, in the actual system, the actual mechanical parameters may differ from the nominal values, and $P_t(s)$ and $P_m(s)$ cannot be considered static under high precision requirements.

2.3. Formulation of Factors Causing Incomplete Decoupling

As Figure 3b shows, due to errors in manufacturing and assembly, the CoM of the mover no longer coincides with the target point, and the actual installation positions of the motors have also changed. In this situation, the actual rigid body dynamic would no longer be equal to the nominal rigid body dynamic (3), which can be expressed as (6):

$$P(s) = \begin{bmatrix} P_{11}(s) & P_{12}(s) & P_{13}(s) \\ P_{21}(s) & P_{22}(s) & P_{23}(s) \\ P_{31}(s) & P_{32}(s) & P_{33}(s) \end{bmatrix}. \quad (6)$$

where the elements can be detailed as

$$\left\{ \begin{array}{l} P_{11}(s) = \frac{J_x J_y + x_0(x_0 - x_1)mJ_x + y_0(y_0 - y_1)mJ_y}{mJ_x J_y s^2} \\ P_{12}(s) = \frac{J_x J_y + x_0(x_0 - x_2)mJ_x + y_0(y_0 - y_2)mJ_y}{mJ_x J_y s^2} \\ P_{13}(s) = \frac{J_x J_y + x_0(x_0 - x_3)mJ_x + y_0(y_0 - y_3)mJ_y}{mJ_x J_y s^2} \\ P_{21}(s) = -\frac{y_0 - y_1}{J_x s^2} \\ P_{22}(s) = -\frac{y_0 - y_2}{J_x s^2} \\ P_{23}(s) = -\frac{y_0 - y_3}{J_x s^2} \\ P_{31}(s) = \frac{x_0 - x_1}{J_y s^2} \\ P_{32}(s) = \frac{x_0 - x_2}{J_y s^2} \\ P_{33}(s) = \frac{x_0 - x_3}{J_y s^2} \end{array} \right. \quad (7)$$

It is evident that the actual plant cannot be completely decoupled with the nominal decoupling matrix, unless the following equations are satisfied:

$$\left\{ \begin{array}{l} x_0 = 0 \\ y_0 = 0 \\ x_1 = 0 \\ y_1 = -l_1 \\ x_2 = l_2 \\ y_2 = l_3 \\ x_3 = -l_2 \\ y_3 = l_3 \end{array} \right. \quad (8)$$

Although the actual system with a nominal decoupling matrix can maintain stability in the case of small errors, it is difficult to obtain the desired performance. Therefore, the decoupling matrix should be improved to enhance the level of decoupling. To decouple the actual rigid body model, the optimal static decoupling matrix can be obtained based on accurate mechanical parameters, such as x_i and y_i , for $i = 0, 1, 2, 3$. However, under the requirements of high speed and high-precision accuracy, the motor dynamics and the transmission delays cannot be neglected. As depicted in Figure 4, with the same coil current input, the static output forces of different motors in different displacements are not constant.

Further considering the effect of the motor time constant, the dynamic model of the motor can be expressed as follows:

$$P_m(s) = \begin{bmatrix} \frac{g_1(y_{v,1})}{\alpha_1 s + 1} & 0 & 0 \\ 0 & \frac{g_2(y_{v,2})}{\alpha_2 s + 1} & 0 \\ 0 & 0 & \frac{g_3(y_{v,3})}{\alpha_3 s + 1} \end{bmatrix} \tag{9}$$

where $y_{v,i}$ is the i -th element of y_v . $g_i(y_{v,i})$ for $i = 1, 2, 3$, which indicates that the force constant of the motor is related to the displacement of the motor.

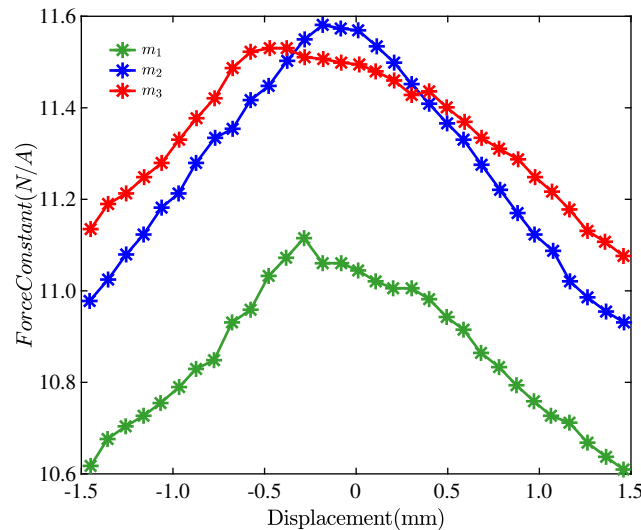


Figure 4. The measured force constants for different motors at different displacements.

On the other hand, the transmission delays matrix can be expressed in detail as

$$P_t(s) = \begin{bmatrix} e^{-\beta_1 s} & 0 & 0 \\ 0 & e^{-\beta_2 s} & 0 \\ 0 & 0 & e^{-\beta_3 s} \end{bmatrix} \tag{10}$$

where β_i for $i = 1, 2, 3$ represents the delays of different transmission channels.

It can be claimed that, if and only if the following conditions are satisfied, the actual plant can be decoupled by a static decoupling matrix. According to the conditions, Theorem 1 can be established.

$$\begin{cases} g_1, g_2, g_3 = const \\ \alpha_1 = \alpha_2 = \alpha_3 \\ \beta_1 = \beta_2 = \beta_3 \end{cases} \tag{11}$$

Theorem 1. Suppose that controlled plant can be represented as $G(s) = P(s)P_m(s)P_t(s)$, where $P(s)$, $P_m(s)$ and $P_t(s)$ are in the form of (6), (9), and (10), respectively. Then, if $G(s)$ can be completely decoupled by a static decoupling matrix, the condition (11) must be satisfied.

Proof. Using proof by contradiction, we suppose that there exists a constant matrix K such that $G(s)K$ is diagonal, and this can be expressed as

$$D(s) = G(s)K = \begin{bmatrix} d_1(s) & 0 & 0 \\ 0 & d_2(s) & 0 \\ 0 & 0 & d_3(s) \end{bmatrix} \tag{12}$$

where the j -row elements of $D(s)$ can be given as

$$D_j(s) = G_j(s)K = \underbrace{[0, \dots, 0]_{j-1}}_{j-1}, d_j(s), \underbrace{[0, \dots, 0]_{n-j}}_{n-j}. \tag{13}$$

We denote $\hat{k}_{j,i}$ as the element in the j -th row and i -th column of the inverse matrix of K . Then, $G_j(s)$ can be written as

$$\begin{aligned} G_j(s) &= D_j(s)K^{-1} \\ &= [0, \dots, 0, d_j(s), 0, \dots, 0]K^{-1}. \\ &= d_j(s)[\hat{k}_{j,1}, \hat{k}_{j,2}, \dots, \hat{k}_{j,n}] \end{aligned} \tag{14}$$

We suppose that $d_j(s)$ can be expressed as $d_j(s) = \frac{a_j(s)}{b_j(s)}$, where $a_j(s)$ and $b_j(s)$ are coprime polynomials and $b_j(s)$ is monic. From (6), the actual rigid body model can be simplified:

$$P(s) = \frac{1}{s^2} \begin{bmatrix} p_{11} & p_{12} & p_{13} \\ p_{21} & p_{22} & p_{23} \\ p_{31} & p_{32} & p_{33} \end{bmatrix}. \tag{15}$$

Subsequently, the j -th row of $G(s)$ can also be determined as

$$\begin{aligned} G_j(s) &= P_j(s)P_m(s)P_t(s) \\ &= \frac{1}{s^2} e^{-\beta_1 s} \left[\frac{p_{j1}g_1(y_{v,1})}{\alpha_1 s + 1}, \frac{p_{j2}g_2(y_{v,2})}{\alpha_2 s + 1} e^{(\beta_1 - \beta_2)s}, \frac{p_{j3}g_3(y_{v,3})}{\alpha_3 s + 1} e^{(\beta_1 - \beta_3)s} \right] \end{aligned} \tag{16}$$

where $P_j(s)$ is the row vector consisting of the elements of the j -th row of $P(s)$.

Comparing (14) and (16), the conditions (11) can be directly obtained. \square

Therefore, to achieve full decoupling of the actual system with motor dynamics and transmission delays, the static decoupling matrix should be substituted by a dynamic decoupling controller. Based on the above analysis, the ideal dynamic decoupling controller can be determined as the following form:

$$K(s) = P_t^{-1}(s)P_m^{-1}(s)K_s. \tag{17}$$

In order to obtain a parameterized model that is easy to handle, two simplification treatments are applied to $P_m^{-1}(s)$ and $P_t^{-1}(s)$. First, the variant force constants $g_i(y_{v,i})$ are approximated as polynomials $\bar{g}_i(y_{v,i})$ of order of m for $i = 1, 2, 3$. $\bar{g}_i(y_{v,i})$ can be written as

$$\bar{g}_i(y_{v,i}(t)) = \gamma_0^i + \gamma_1^i y_{v,i}(t) + \dots + \gamma_m^i y_{v,i}^m(t) \tag{18}$$

where $y_{v,i}^j(t)$ represents the j -th power of $y_{v,i}(t)$ and $\gamma_j^i \in R$ for $j = 0, \dots, m$ are unknown coefficients. Then the inverse of $P_m(s)$ can be approximated as

$$\hat{P}_m(s) = \begin{bmatrix} \frac{\alpha_1 s + 1}{\bar{g}_1(y_{v,1})} & 0 & 0 \\ 0 & \frac{\alpha_2 s + 1}{\bar{g}_2(y_{v,2})} & 0 \\ 0 & 0 & \frac{\alpha_3 s + 1}{\bar{g}_3(y_{v,3})} \end{bmatrix}. \tag{19}$$

Second, to obtain an invertible approximation of the pure delays term of $P_t(s)$, the Pade approximant [24] can be utilized, and the inverse of $P_t(s)$ can be written approximately as

$$\hat{P}_t(s) = \begin{bmatrix} \beta_1 s + 1 & 0 & 0 \\ 0 & \beta_2 s + 1 & 0 \\ 0 & 0 & \beta_3 s + 1 \end{bmatrix}. \tag{20}$$

Finally, to ensure the causality of the dynamic decoupling controller, a Q-filter with a relative order of 2 is required, and the desired dynamic decoupling controller based on the compensation of motor dynamics and transmission delays can be parameterized as

$$K(s) = Q(s)\hat{P}_t(s)\hat{P}_m(s)K_s \tag{21}$$

$$= \begin{bmatrix} \frac{(\alpha_1 s + 1)(\beta_1 s + 1)}{\bar{g}_1(y_{v,1})L(s)} & 0 & 0 \\ 0 & \frac{(\alpha_2 s + 1)(\beta_2 s + 1)}{\bar{g}_2(y_{v,2})L(s)} & 0 \\ 0 & 0 & \frac{(\alpha_3 s + 1)(\beta_3 s + 1)}{\bar{g}_3(y_{v,3})L(s)} \end{bmatrix} \begin{bmatrix} k_{11} & k_{12} & k_{13} \\ k_{21} & k_{22} & k_{23} \\ k_{31} & k_{32} & k_{33} \end{bmatrix}$$

where $L(s)$ is a known second-order stable polynomial in the s domain. As mentioned above, the unknown parameters of $K(s)$ can be determined based on the mechanical parameters, motor dynamics, and transmission delays. However, it is difficult to measure and identify these parameters, and additional errors will be introduced in the final calculation process. To address these problems, an on-line optimization method is developed.

3. Data-Driven Optimization Method

In this section, a data-driven method is proposed to estimate the unknown parameters of the dynamic decoupling controller $K(s)$. The configuration of the proposed method is depicted in Figure 5. As shown in Figure 5, a reference model is used which should be diagonal, and the essential idea is to adjust the parameters of $K(s)$ to make the decoupled system as close to $\tilde{D}(s)$ as possible.

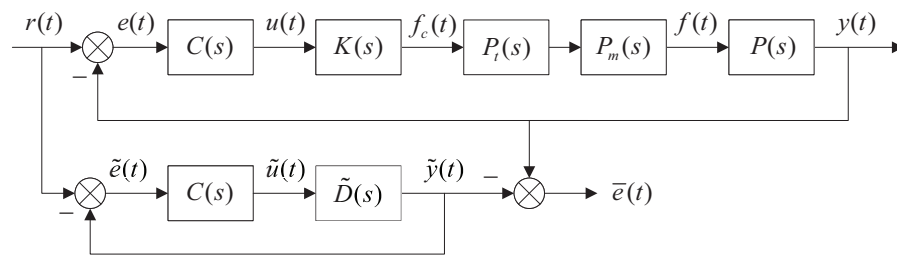


Figure 5. Block diagram of the proposed data-driven optimization method.

In other words, if the output of $\tilde{D}(s)$ is equal to the output of $G(s)K(s)$ with the same conditions of reference input and feedback controller, then $\tilde{D}(s) = G(s)K(s)$ can be achieved. We suppose that the output of the reference model is equal to $y(t)$; the output of the feedback controller in reference model can be determined as

$$y(t) = \tilde{D}(s)\tilde{u}(s). \tag{22}$$

From (22), if the output of the feedback controller $u(t)$ in the actual system can be equal to $\tilde{u}(t)$ by adjusting the parameters of $K(s)$, the following equations can be established:

$$\begin{aligned} \tilde{D}(s)\tilde{u}(s) &= G(s)K(s)u(t) \\ \tilde{D}(s) &= G(s)K(s) \end{aligned} \tag{23}$$

It is obvious that the decoupled system is completely diagonal if (23) is satisfied. Therefore, the following equivalent objective function can be established, and the optimal estimate of the parameters of $K(s)$ can be obtained by minimizing it:

$$K^*(s) = \arg \min_{K(s)} J = \arg \min_{K(s)} \|f_c(t) - K(s)\tilde{u}(t)\|_2^2. \tag{24}$$

where $\|x\|_2$ denotes the l_2 -norm of vector x .

Substituting (21) into (24), the objective function J can be derived as

$$\begin{aligned}
 J &= \|f_c(t) - Q(s)\hat{P}_t(s)\hat{P}_m(s)K_s\tilde{u}(t)\|_2^2 \\
 &= \sum_{i=1}^3 \|f_{c,i}(t) - Q(s)\hat{P}_{t,i}(s)\hat{P}_m(s)K_s\tilde{u}(t)\|_2^2 \\
 &= \sum_{i=1}^3 J_i
 \end{aligned} \tag{25}$$

where $f_{c,i}$ represents the i -th element of f_c . $\hat{P}_{t,i}(s)$ denotes a row vector consisting of the i -th row elements of $\hat{P}_t(s)$. Then, the optimization of J can be achieved by optimizing J_1, J_2 , and J_3 , respectively.

Substituting (21) into (25), J_i can be parameterized as follows:

$$\begin{aligned}
 J_i &= \|f_{c,i}(t) - Q(s)\hat{P}_{t,i}(s)\hat{P}_m(s)K_s\tilde{u}(t)\|_2^2 \\
 &= \|f_{c,i}(t) - \frac{(\alpha_i s + 1)(\beta_i s + 1)}{\bar{g}_i(y_{v,i})L(s)} \sum_{j=1}^3 k_{ij}\tilde{u}_j(t)\|_2^2 \\
 &= \left\| \frac{1}{\bar{g}_i(y_{v,i})} (\bar{g}_i(y_{v,i})f_{c,i}(t) - \frac{(\alpha_i s + 1)(\beta_i s + 1)}{L(s)} \sum_{j=1}^3 k_{ij}\tilde{u}_j(t)) \right\|_2^2
 \end{aligned} \tag{26}$$

where $\hat{P}_{t,i}(s)$ denotes the i -th row of $\hat{P}_t(s)$. Since g_i is not equal to 0 and fluctuates less around the nominal value and the minimum of J_i depends on the error term in (26), the minimization of J_i can be equivalent to the minimization of \bar{J}_i , which can be written as

$$\bar{J}_i = \left\| \bar{g}_i(y_{v,i})f_{c,i}(t) - \frac{(\alpha_i s + 1)(\beta_i s + 1)}{L(s)} \sum_{j=1}^3 k_{ij}\tilde{u}_j(t) \right\|_2^2 \tag{27}$$

Substituting (18) into (27), the objective function can be further derived as

$$\bar{J}_i = \left\| (\gamma_0^i + \gamma_1^i y_{v,i}(t) + \dots + \gamma_m^i y_{v,i}^m(t))f_{c,i}(t) - \frac{(\alpha_i s + 1)(\beta_i s + 1)}{L(s)} \sum_{j=1}^3 k_{ij}\tilde{u}_j(t) \right\|_2^2 \tag{28}$$

For the simplicity of expression, we define the following symbols:

$$\left\{ \begin{aligned}
 h_{i,j}(t) &= y_{v,i}^j(t)f_{c,i}(t) \\
 q_j^2(t) &= \frac{s^2}{L(s)}\tilde{u}_j(t) \\
 q_j^1(t) &= \frac{s}{L(s)}\tilde{u}_j(t) \\
 q_j^0(t) &= \frac{1}{L(s)}\tilde{u}_j(t) \\
 \theta_{i,j}^3 &= \frac{\gamma_j^i}{\gamma_0^i} \\
 \theta_{i,j}^2 &= \frac{\alpha_i\beta_i k_{ij}}{\gamma_0^i} \\
 \theta_{i,j}^1 &= \frac{(\alpha_i + \beta_i)k_{ij}}{\gamma_0^i} \\
 \theta_{i,j}^0 &= \frac{k_{ij}}{\gamma_0^i}
 \end{aligned} \right. \tag{29}$$

Subsequently, (28) can be simplified as

$$\bar{J}_i = \frac{1}{(\gamma_0^i)^2} \|h_{i,0}(t) + \sum_{j=1}^m \theta_{i,j}^3 h_{i,j}(t) - \sum_{j=1}^3 \theta_{i,j}^2 q_j^2(t) - \sum_{j=1}^3 \theta_{i,j}^1 q_j^1(t) - \sum_{j=1}^3 \theta_{i,j}^0 q_j^0(t)\|_2^2. \quad (30)$$

To solve the optimization problem in practice, (30) should be converted to a discrete form

$$\bar{J}_i = \frac{1}{N} \sum_{k=1}^N \frac{1}{(\gamma_0^i)^2} \|h_{i,0}(k) + \sum_{j=1}^m \theta_{i,j}^3 h_{i,j}(k) - \sum_{j=1}^3 \theta_{i,j}^2 q_j^2(k) - \sum_{j=1}^3 \theta_{i,j}^1 q_j^1(k) - \sum_{j=1}^3 \theta_{i,j}^0 q_j^0(k)\|_2^2 \quad (31)$$

where $h_{i,j}(k)$, $q_j^2(k)$, $q_j^1(k)$, and $q_j^0(k)$ are the k -th sampling values of $h_{i,j}(t)$, $q_j^2(t)$, $q_j^1(t)$, and $q_j^0(t)$, respectively and N is the sampling number. For simplicity, we define

$$\begin{cases} T^i = [h_{i,0}(1), h_{i,0}(2), \dots, h_{i,0}(N)]^T \in R^N \\ \phi^i(k) = [h_{i,1}(k), h_{i,2}(k), \dots, h_{i,m}(k), q_1^2(k), q_2^2(k), q_3^2(k), \\ \quad q_1^1(k), q_2^1(k), q_3^1(k), q_1^0(k), q_2^0(k), q_3^0(k)]^T \in R^{m+9} \\ \Phi^i = [\phi^i(1), \phi^i(2), \dots, \phi^i(N)]^T \in R^{N \times (m+9)} \\ \eta_i^3 = [\theta_{i,1}^3, \theta_{i,2}^3, \dots, \theta_{i,m}^3]^T \in R^m \\ \eta_i^2 = [\theta_{i,1}^2, \theta_{i,2}^2, \theta_{i,3}^2]^T \in R^3 \\ \eta_i^1 = [\theta_{i,1}^1, \theta_{i,2}^1, \theta_{i,3}^1]^T \in R^3 \\ \eta_i^0 = [\theta_{i,1}^0, \theta_{i,2}^0, \theta_{i,3}^0]^T \in R^3 \\ \Omega^i = [-(\eta_i^3)^T, (\eta_i^2)^T, (\eta_i^1)^T, (\eta_i^0)^T]^T \in R^{m+9} \end{cases} \quad (32)$$

Substituting (32) into (31), the objective function can be rewritten as

$$\bar{J}_i = \frac{1}{N(\gamma_0^i)^2} \|T^i - \Phi^i \Omega^i\|_2^2. \quad (33)$$

Then, the estimate of Ω^i can be obtained by using the least square method as follows:

$$\hat{\Omega}^i = ((\Phi^i)^T (\Phi^i))^{-1} (\Phi^i)^T T^i. \quad (34)$$

The estimate of $\theta_{i,j}^3$, $\theta_{i,j}^2$, $\theta_{i,j}^1$, and $\theta_{i,j}^0$ can easily obtained based on (29), which can be denoted as $\hat{\theta}_{i,j}^3$, $\hat{\theta}_{i,j}^2$, $\hat{\theta}_{i,j}^1$, and $\hat{\theta}_{i,j}^0$. In addition, the estimate of $\alpha_i \beta_i$, $\alpha_i + \beta_i$ and $g_i(y_{v,i}) / \gamma_0^i$ can be obtained as $\hat{\tau}_i^2$, $\hat{\tau}_i^1$, and $\hat{g}_i(y_{v,i})$, which can be written as

$$\begin{cases} \hat{\tau}_i^2 = [(\hat{\eta}_i^0)^T \hat{\eta}_i^0]^{-1} (\hat{\eta}_i^0)^T \hat{\eta}_i^2 \\ \hat{\tau}_i^1 = [(\hat{\eta}_i^1)^T \hat{\eta}_i^1]^{-1} (\hat{\eta}_i^1)^T \hat{\eta}_i^1 \\ \hat{g}_i(y_{v,i}) = 1 + \hat{\theta}_{i,1}^3 y_{v,i}(t) + \dots + \hat{\theta}_{i,m}^3 y_{v,i}^m(t) \end{cases} \quad (35)$$

Finally, the estimate of $K(s)$ can be expressed as

$$\hat{K}(s) = \begin{bmatrix} \frac{\hat{\tau}_1^2 s^2 + \hat{\tau}_1^1 s + 1}{\hat{g}(y_{v,1})L(s)} & 0 & 0 \\ 0 & \frac{\hat{\tau}_2^2 s^2 + \hat{\tau}_2^1 s + 1}{\hat{g}(y_{v,2})L(s)} & 0 \\ 0 & 0 & \frac{\hat{\tau}_3^2 s^2 + \hat{\tau}_3^1 s + 1}{\hat{g}(y_{v,3})L(s)} \end{bmatrix} \begin{bmatrix} \hat{\theta}_{11}^0 & \hat{\theta}_{12}^0 & \hat{\theta}_{13}^0 \\ \hat{\theta}_{21}^0 & \hat{\theta}_{22}^0 & \hat{\theta}_{23}^0 \\ \hat{\theta}_{31}^0 & \hat{\theta}_{32}^0 & \hat{\theta}_{33}^0 \end{bmatrix} \quad (36)$$

4. Simulations Results

In this section, the effectiveness of the proposed method is validated by comparing it with the nominal decoupling method and the ideal static decoupling method, which can decouple the rigid body model of the system in the absence of the motor dynamics and transmission delays. These methods can be represented as follows:

- (1) M_0 : the nominal static decoupling control method.
- (2) M_1 : the ideal static decoupling control method.
- (3) M_2 : the proposed dynamic decoupling control method.

The static decoupling matrices obtained by M_1 and M_1 are denoted as K_0 and K_1 , respectively. The dynamic decoupling controller determined by M_2 is represented as $K_2(s)$.

4.1. Simulation Setup

A simulation experiment was conducted to demonstrate the effectiveness of M_2 and the simulation block diagram was established, as Figure 6 shows. A fixed step size of 0.0002 was adopted in the numerical calculations of differential equations, and the algorithm of the solver was set to ode4. The total simulation time was set to 1 s, which meant that the sampling number was 5000. The actual values of mechanical parameters in the coordinate C_{xyz} are provided in Table 1. We supposed that the mass of the SS stage was $m = 20$ kg and the moment of inertia of θ_x and θ_y at the CoM were $J_x = 0.33$ kg · m and $J_y = 0.45$ kg · m, respectively. By the rigid body hypothesis, the transfer function model between the driving forces of motors and the three DoFs' displacement of the target point can be given as

$$P(s) = \begin{bmatrix} \frac{0.05367}{s^2} & \frac{0.04523}{s^2} & \frac{0.04987}{s^2} \\ \frac{0.3333}{s^2} & \frac{0.2879}{s^2} & \frac{0.2576}{s^2} \\ \frac{0.03333}{s^2} & -\frac{0.1889}{s^2} & \frac{0.2444}{s^2} \end{bmatrix}. \tag{37}$$

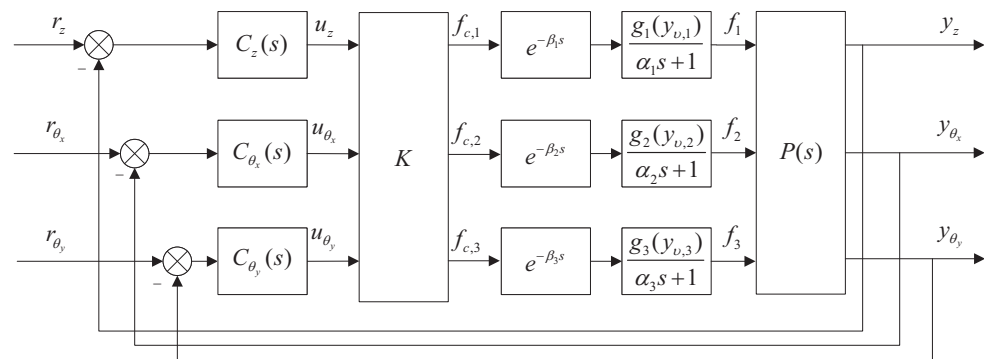


Figure 6. The diagram of the simulation experiment.

Table 1. Actual mechanical parameters used in the simulation.

Points	Values (m)
(x_0, y_0)	$(0.01, 0.01)$
(x_1, y_1)	$(-0.005, -0.1)$
(x_2, y_2)	$(0.095, 0.105)$
(x_3, y_3)	$(-0.1, 0.095)$

The nominal mechanical parameters presented in Figure 3a are $l_1 = 0.1m$, $l_2 = 0.1m$, and $l_3 = 0.1m$. Based on the nominal mechanical parameters, the nominal static decoupling matrix K_0 can be determined as

$$K_0 = \begin{bmatrix} 0.5 & -5.0 & 0 \\ 0.25 & 2.5 & -5.0 \\ 0.25 & 2.5 & 5.0 \end{bmatrix}. \tag{38}$$

We specify the desired decoupled model as follows:

$$D(s) = \begin{bmatrix} \frac{0.05}{s^2} & 0 & 0 \\ 0 & \frac{3.0303}{s^2} & 0 \\ 0 & 0 & \frac{2.2222}{s^2} \end{bmatrix}. \quad (39)$$

Based on the actual rigid body model of the plant and the desired decoupled model, the ideal static decoupling matrix K_1 can be determined as

$$K_1 = \begin{bmatrix} 0.4535 & -4.7284 & -0.4581 \\ 0.3432 & 2.6454 & -5.1557 \\ 0.2033 & 2.6890 & 5.1694 \end{bmatrix}. \quad (40)$$

To investigate the effect of motor dynamics and transmission delays, the dynamic equations in the form of (9) and (10) were added into the simulation. The parameters used are listed in Tables 2 and 3. In the simulation, the variant force constants for different motors were approximated as a polynomial of order 5, according to the measurement data shown in Figure 4. Because these parameters were close to the nominal values, the diagonal dominance of the system could still be ensured by using the nominal static decoupling method when these errors were ignored. Thus, a decentralized controller $C(s)$ could be designed to ensure the stability of the system. Nevertheless, due to the inaccurate mechanical parameters, there would have been a great deterioration of performance. To improve the performance of the precision mechatronic system, the dynamic decoupling method proposed in Section 3 can be utilized. In order to estimate the unknown parameters of the dynamic decoupling controller, a data-driven optimization method M_2 is developed in Section 4.

Table 2. Actual parameters of motor dynamics and transmission delays used in the simulation.

Parameters	Values
α_1	0.002
α_2	0.0018
α_3	0.0021
β_1	0.0002
β_2	0.0001
β_3	0.0003

Table 3. Parameters of the force constant polynomial used in the simulation.

Parameters (N/m^i)	m_1	m_2	m_3
α_0	11.05	11.54	11.50
α_1	-97.35	-108.42	-150.54
α_2	-3.47×10^5	-4.67×10^5	-2.30×10^5
α_3	1.11×10^8	6.88×10^7	1.38×10^8
α_4	7.02×10^{10}	9.44×10^{10}	2.26×10^{10}
α_5	-3.28×10^{13}	-1.30×10^{13}	-3.73×10^{13}

To estimate the unknown parameters in M_2 , the reference $\tilde{D}(s)$ model was selected as $D(s)$, and the order used in (18) was chosen as $m = 2$ in the simulation. By conducting excitation experiments on the closed-loop system using K_0 , the dynamic decoupling controller $K_2(s)$ could be determined. The estimated results are shown in Table 4 with the Q-filter selected as follows:

$$Q(s) = \frac{1}{7.036 \times 10^{-6}s^2 + 0.003751s + 1} \quad (41)$$

Table 4. The estimated results based on the structure of dynamic decoupling controller.

Parameters	Estimate	Parameters	Estimate	Parameters	Estimate
$\hat{\tau}_1^2$	4.159×10^{-7}	$\hat{\tau}_2^2$	1.909×10^{-7}	$\hat{\tau}_3^2$	6.698×10^{-7}
$\hat{\tau}_1^1$	0.002198	$\hat{\tau}_2^1$	0.0019	$\hat{\tau}_3^1$	0.002393
$\hat{\theta}_{11}^0$	0.4718	$\hat{\theta}_{12}^0$	-4.9611	$\hat{\theta}_{13}^0$	-0.6164
$\hat{\theta}_{21}^0$	0.3421	$\hat{\theta}_{22}^0$	2.2755	$\hat{\theta}_{23}^0$	-5.3083
$\hat{\theta}_{31}^0$	0.2033	$\hat{\theta}_{32}^0$	3.0487	$\hat{\theta}_{33}^0$	5.2963
$\hat{\theta}_{1,1}^0$	-8.4778	$\hat{\theta}_{1,2}^0$	-30,359		
$\hat{\theta}_{2,1}^0$	-9.7282	$\hat{\theta}_{2,2}^0$	-41,652		
$\hat{\theta}_{3,1}^0$	-12.7135	$\hat{\theta}_{3,2}^0$	-21,208		

4.2. Performance Assessment

To demonstrate the effectiveness of the dynamic decoupling method more intuitively, some validation experiments in the time domain were carried out. Tracking experiments for three DoFs were conducted for different systems with the same feedback controller. In the first tracking experiment, a step signal of 100 μm was exerted in z -DoF as the reference input. Similarly, a step signal of 100 μrad was exerted in θ_x -DoF and θ_y -DoF as the reference input in the second and the third tracking experiments, respectively. It should be noted that in each tracking experiment, the reference inputs of the other two DoFs were set as 0, except the one tracking the step signal. Therefore, the output responses of these DoFs should be 0 when the system is fully decoupled. However, the outputs of the DOFs that track the zero signal were much greater than 0 when using M_0 and M_1 as shown in Figures 7–9. The outputs were derived from the inaccurate decoupling, which can be referred to as the cross-talk. On the contrary, the cross-talk of the decoupled system using M_2 was almost negligible. It can be concluded that the decoupling effect of the M_2 was the best. Consequently, to quantify the degree of decoupling, the sum of the maximum value of cross-talk can be used as the indicator, which can be denoted as

$$SAC = \sum_{i=z} \sum_{j \neq i} W_{ji} |e_{j,i}| \quad (42)$$

where i, j are selected in the set of $\{z, \theta_x, \theta_y\}$, respectively, W_{ji} is the weighting coefficient, and $e_{j,i}$ represents the maximum value of the cross-talk of the j -DoF when the i -DoF is excited. Based on the maximum value of cross-talk in tracking experiments shown in Table 5, the SAC of different decoupled systems using different decoupling methods can be determined as

$$\begin{cases} SAC_1 = 1.2799 \times 10^{-4} \\ SAC_2 = 2.7684 \times 10^{-5} \\ SAC_3 = 2.5791 \times 10^{-7} \end{cases} \quad (43)$$

where the weighting coefficient is chosen as $W_{ji} = 1$ for $i, j \in \{z, \theta_x, \theta_y\}$. SAC_1 , SAC_2 , and SAC_3 are calculated based on the decoupled system with K_0 , K_1 , and $K_2(s)$, respectively. It can be concluded that the dynamic decoupling method proposed in this paper outperforms the other two static decoupling methods, and at least 99.46% and 97.75% performance improvements were obtained compared to M_1 and M_2 , respectively. Consequently, the effectiveness and the superiority of the proposed method can be clearly demonstrated.

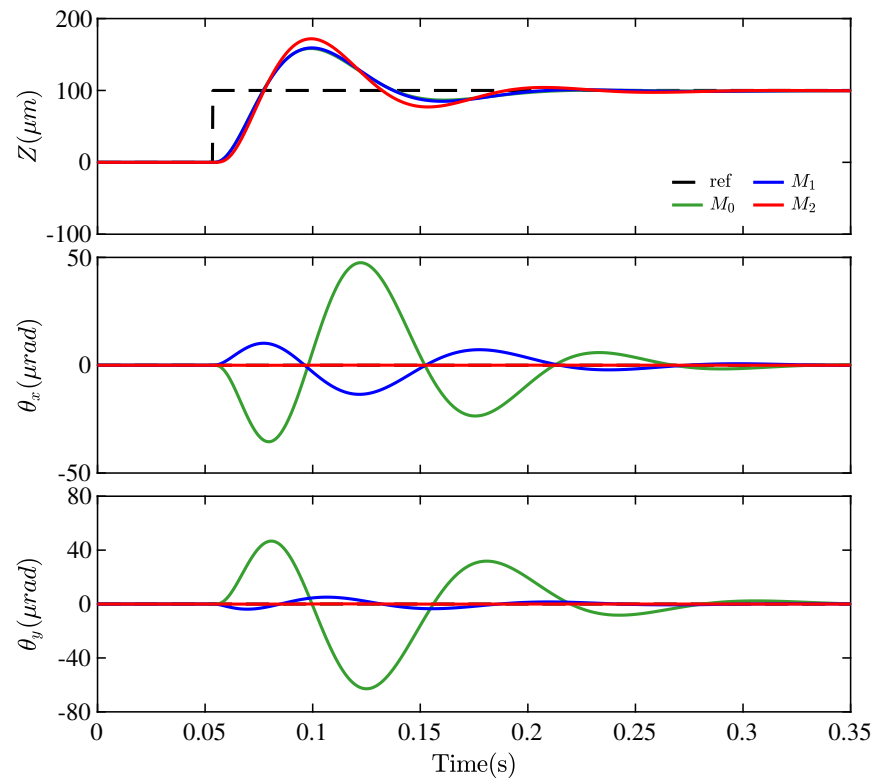


Figure 7. The output responses of tracking experiment of z-DoF.

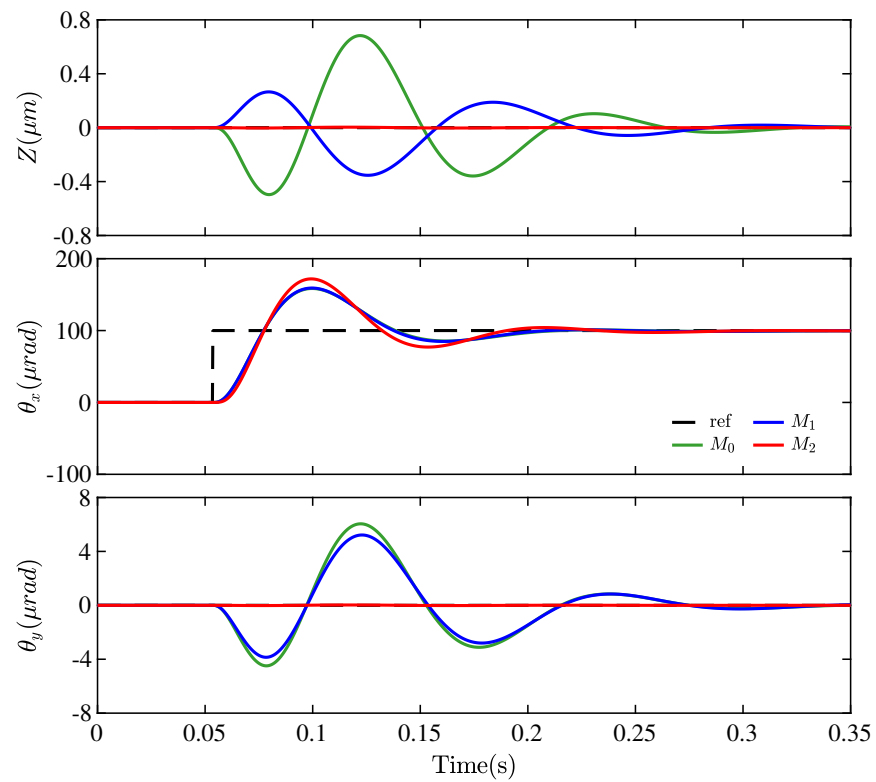


Figure 8. The output responses of tracking experiment of θ_x -DoF.

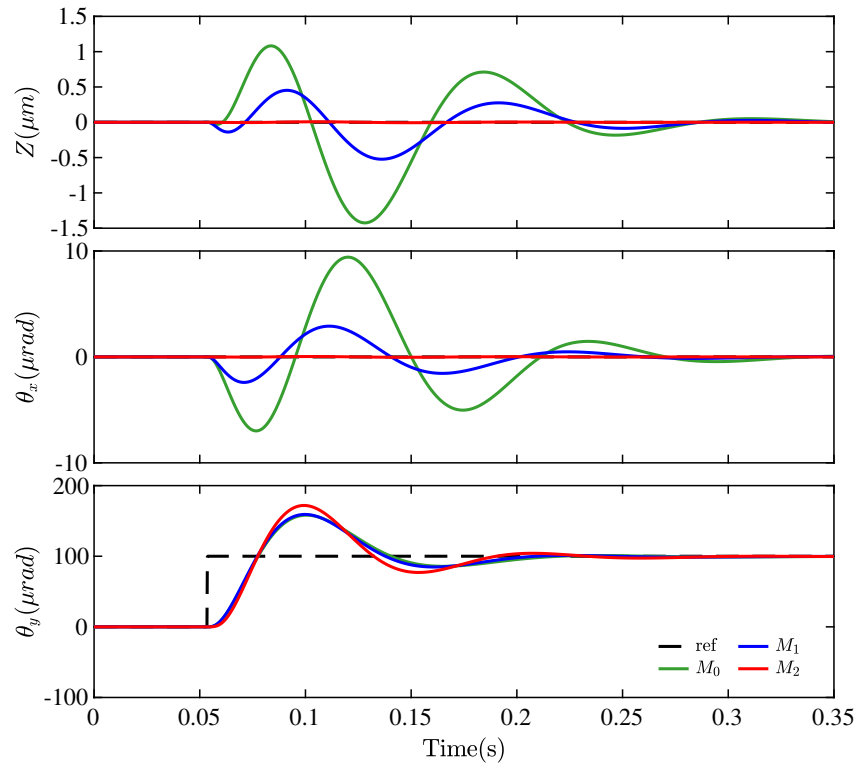


Figure 9. The output responses of tracking experiment of θ_y -DoF.

Table 5. The maximum value of cross-talk in tracking experiments with different decoupling controllers (matrix).

Excitated DoF	e_z (μm)	e_{θ_x} (μrad)	e_{θ_y} (μrad)
z	None ¹	47.53	62.87
	None	13.58	5.096
	None	0.07180	0.1148
θ_x	0.6832	None	6.056
	0.3564	None	5.220
	0.003698	None	0.02546
θ_y	1.430	9.417	None
	0.5249	2.902	None
	0.007016	0.03507	None

¹ "None" indicates that the data is not relevant to the content of the text.

5. Conclusions

In this paper, a novel dynamic decoupling method was developed based on the compensation for varying motor dynamics and transmission delays. The key essence of the proposed method lies in the structured dynamic component included in the decoupling controller. What is more, to estimate the unknown parameters, an on-line data-driven optimization algorithm was presented, where only inputs and outputs of the plant need to be measured in a single experiment. Both theoretical analysis and experimental results confirm that the proposed structured dynamic decoupling approach can achieve accurate decoupling; thus, the interactions between multiple DOFs in the mechatronic system can be eliminated significantly. Consequently, compared to the conventional static decoupling methods, a 97.75% performance improvement can be obtained by the proposed dynamic decoupling method.

Author Contributions: Conceptualization, K.L.; methodology, K.L.; writing—original draft, K.L. and F.S.; software, K.L.; validation, K.L.; investigation, K.L. and Y.L.; supervision, Y.L. and J.T.; project administration, Y.L. and J.T. All authors have read and agreed to the published version of the manuscript.

Funding: This research was funded by the National Natural Science Foundation of China (52075132 and 52105546) and the Opening Foundation of State Key Lab of Digital Manufacturing Equipment & Technology, China (DMETKF2020024).

Data Availability Statement: All data used are contained within the article.

Conflicts of Interest: The authors declare no conflicts of interest.

Abbreviations

The following abbreviations are used in this manuscript:

CoM	Center of mass
DoF	Degree of freedom
DoFs	Degrees of freedom
ETF	Equivalent transfer function
MIMO	Multiple-input multiple output
SAC	Sum of the absolute value of the maximum value of cross-talk
SISO	Single-input single-output
VRFT	Virtual reference feedback tuning

References

1. Incremona, G.P.; Ferrara, A.; Magni, L. MPC for Robot Manipulators With Integral Sliding Modes Generation. *IEEE-ASME Trans. Mechatron.* **2017**, *3*, 1299–1307. [\[CrossRef\]](#)
2. Zheng, Y.; Zhou, Z.; Huang, H. A multi-frequency MIMO control method for the 6DOF micro-vibration exciting system. *Acta Astronaut.* **2020**, *170*, 552–569. [\[CrossRef\]](#)
3. Hanifzadegan, M.; Nagamune, R. Contouring Control of CNC Machine Tools Based on Linear Parameter-Varying Controllers. *IEEE-ASME Trans. Mechatron.* **2016**, *5*, 2522–2530. [\[CrossRef\]](#)
4. Jeon, T.; Kim, D.; Song, Y.; Paek, I. Design and Validation of Demanded Power Point Tracking Control Algorithm for MIMO Controllers in Wind Turbines. *Energies* **2021**, *18*, 5818. [\[CrossRef\]](#)
5. Ma, J.; Cheng, Z.; Zhu, H.; Li, X.; Tomizuka, M.; Lee, T.H. Convex Parameterization and Optimization for Robust Tracking of a Magnetically Levitated Planar Positioning System. *IEEE Trans. Ind. Electron.* **2022**, *4*, 3798–3809. [\[CrossRef\]](#)
6. Song, F.; Liu, Y.; Jin, W.; Tan, J.; He, W. Data-Driven Feedforward Learning With Force Ripple Compensation for Wafer Stages: A Variable-Gain Robust Approach. *IEEE Trans. Neural Netw. Learn. Syst.* **2022**, *4*, 1594–1608. [\[CrossRef\]](#) [\[PubMed\]](#)
7. Schitter, G. Advanced Mechatronics for Precision Engineering and Mechatronic Imaging Systems. *IFAC Pap.* **2015**, *1*, 942. [\[CrossRef\]](#)
8. Butler, H. Position Control in Lithographic Equipment An Enabler for Current-Day Chip Manufacturing. *IEEE Control Syst. Mag.* **2011**, *5*, 28–47.
9. Heertjes, M.; Hennekens, D.; Steinbuch, M. MIMO feed-forward design in wafer scanners using a gradient approximation-based algorithm. *Control Eng. Pract.* **2010**, *5*, 495–506. [\[CrossRef\]](#)
10. Barros, C.P.B.; Butler, H.; van de Wijdeven, J.; Tóth, R. On feedforward control of piezoelectric dual-stage actuator systems. In Proceedings of the 2021 60th IEEE Conference on Decision and Control (CDC), Austin, TX, USA, 14–17 December 2021; pp. 5588–5594.
11. Poot, M.; Portegies, J.; Mooren, N.; van Haren, M.; van Meer, M.; Oomen, T. Gaussian Processes for Advanced Motion Control. *IEEJ J. Ind. Appl.* **2022**, *3*, 396–407.
12. Li, B.; Zhou, X.; Ning, Z.; Guan, X.; Yiu, K.-F.C. Dynamic event-triggered security control for networked control systems with cyber-attacks: A model predictive control approach. *Inf. Sci.* **2022**, *612*, 384–398. [\[CrossRef\]](#)
13. Zhao, D.; Xia, L.; Dang, H.; Wu, Z.; Li, H. Design and control of air supply system for PEMFC UAV based on dynamic decoupling strategy. *Energy Convers. Manag.* **2022**, *253*, 115159. [\[CrossRef\]](#)
14. Hagglund, T.; Shinde, S.; Theorin, A.; Thomsen, U. An industrial control loop decoupler for process control applications. *Control. Eng. Pract.* **2022**, *123*, 105138. [\[CrossRef\]](#)
15. Heertjes, M.; van Engelen, A. Minimizing cross-talk in high-precision motion systems using data-based dynamic decoupling. *Control Eng. Pract.* **2011**, *12*, 1423–1432. [\[CrossRef\]](#)
16. Shen, Y.; Cai, W.-J.; Li, S. Normalized decoupling control for high-dimensional MIMO processes for application in room temperature control HVAC systems. *Control Eng. Pract.* **2010**, *6*, 652–664. [\[CrossRef\]](#)

17. Luan, X.; Chen, Q.; Liu, F. Equivalent Transfer Function based Multi-loop PI Control for High Dimensional Multivariable Systems. *Int. J. Control Autom. Syst.* **2015**, *2*, 346–352. [[CrossRef](#)]
18. Wu, G.; Sun, H.; Zhang, X.; Egea-Alvarez, A.; Zhao, B.; Xu, S.; Wang, S.; Zhou, X. Parameter Design Oriented Analysis of the Current Control Stability of the Weak-Grid-Tied VSC. *IEEE Trans. Power Deliv.* **2021**, *3*, 1458–1470. [[CrossRef](#)]
19. Luan, X.; Chen, Q.; Liu, F. Centralized PI control for high dimensional multivariable systems based on equivalent transfer function. *ISA Trans.* **2014**, *5*, 1554–1561. [[CrossRef](#)] [[PubMed](#)]
20. Rahideh, A.; Bajodah, A.H.; Shaheed, M.H. Real time adaptive nonlinear model inversion control of a twin rotor MIMO system using neural networks. *Eng. Appl. Artif. Intell.* **2012**, *6*, 1289–1297. [[CrossRef](#)]
21. van Dael, M.; Witvoet, G.; Swinkels, B.; Oomen, T. Systematic feedback control design for scattered light noise mitigation in Virgo's MultiSAS. In Proceedings of the 2022 IEEE 17th International Conference on Advanced Motion Control (AMC), Padova, Italy, 18–20 February 2022; pp. 300–305.
22. Wang, X.; Yang, B.; Zhu, Y. Optimization of current distribution coefficients to decouple the 6-DOF fine stage of lithographic equipment. *Optik* **2016**, *20*, 9896–9904. [[CrossRef](#)]
23. Campestrini, L.; Eckhard, D.; Gevers, M.; Bazanella, A.S. Virtual Reference Feedback Tuning for non-minimum phase plants. *Automatica* **2011**, *8*, 1778–1784. [[CrossRef](#)]
24. Wang, Y.; Zhang, J.; Zhang, H.; Xie, X. Adaptive Fuzzy Output-Constrained Control for Nonlinear Stochastic Systems with Input Delay and Unknown Control Coefficients. *IEEE Trans. Cybern.* **2021**, *11*, 5279–5290. [[CrossRef](#)] [[PubMed](#)]

Disclaimer/Publisher's Note: The statements, opinions and data contained in all publications are solely those of the individual author(s) and contributor(s) and not of MDPI and/or the editor(s). MDPI and/or the editor(s) disclaim responsibility for any injury to people or property resulting from any ideas, methods, instructions or products referred to in the content.